Photosynthesis in intact Chlamydomonas reinhardtii studied by time-resolved fluorescence spectroscopy

Wlodarczyk, L.M.

2019

document version
Publisher's PDF, also known as Version of record

3

Excitation energy transfer in Chlamydomonas reinhardtii deficient in the PSI core or the PSII core under conditions mimicking state transitions.

This chapter is based on the following publication with the same title:

L.M. Wlodarczyk
E. Dinc
R. Croce
J.P. Dekker

Biochimica et Biophysica Acta (BBA) – Bioenergetics 1857 (2016) 625-633

Abstract

The efficient use of excitation energy in photosynthetic membranes is achieved by a dense network of pigment-protein complexes. These complexes fulfill specific functions and interact dynamically with each other in response to rapidly changing environmental conditions. Here, we studied how in the intact cells of *Chlamydomonas reinhardtii* (*C.r.*) the lack of the photosystem I (PSI) core or the photosystem II (PSII) core affects these interactions. To that end the mutants F15 and M18 (both PSI-deficient) and FUD7 (PSII-deficient) were incubated under conditions known to promote state transitions in wild-type. The intact cells were then instantly frozen to 77 K and the full-spectrum time-resolved fluorescence emission of the cells was measured by means of streak camera. In the PSI-deficient mutants excitation energy transfer (EET) towards light-harvesting complexes of PSI (Lhca) occurs in less than 0.5 ns, and fluorescence from Lhca decays in 3.1 ns. Decreased trapping by PSII and increased fluorescence of Lhca upon state 1 (S1) → state 2 (S2) transition appears in the F15 and less in the M18 mutant. In the PSII-deficient mutant FUD7, quenched (0.5 ns) and unquenched (2 ns) light-harvesting complexes of PSII (LHCII) are present in both states, with the quenched form more abundant in S2 than in S1. Moreover, EET of 0.4 ns from the remaining LHCII to PSI increases upon S1 → S2 transition. We relate the excitation energy kinetics observed in F15, M18 and FUD7 to the remodeling of the photosynthetic apparatus in these mutants under S1 and S2 conditions.

Introduction

Efficient photosynthesis strongly relies on a specific composition and arrangement of the photosynthetic apparatus. The photosynthetic membranes are thus densely packed with different pigment–protein complexes [1] whose main functions are to harvest light, and to perform photochemistry [2]. The former role is realized by so-called light harvesting antennae which contain a high concentration of chlorophylls (Chls) and carotenoids [3]. The antennae of higher plants and algae consist of the Lhcb and Lhca proteins (for characterization in *Chlamydomonas reinhardtii*, see [4] and [5], respectively). The former include major light-harvesting complexes (LHCII), which can serve as antenna of photosystem II (PSII) and of photosystem I (PSI), the minor antennae CP26 and CP29 present both in higher plants and in *Chlamydomonas reinhardtii* (*C.r.*), as well as CP24 present solely in higher plants [6]. The Lhca proteins act as PSI antennae, although it has been suggested previously that in *C.r.* mutants lacking the PSI core they can also transfer excitation energy to PSII [7,8]. The photochemistry takes place in a photochemical reaction center, present in the cores of both PSI and PSII, and it ultimately results in electron transport and in a proton gradient across the photosynthetic membranes, both utilized in the further steps of photosynthesis [9].

In the present work we study the earliest event in photosynthesis, namely excitation energy transfer (EET) from the light-harvesting antennae to the reaction centers, in the green alga *Chlamydomonas reinhardtii*. We measured full-spectrum time-resolved fluorescence in mutants of *C.r.* deficient in the PSI core (F15 and M18) or the PSII core (FUD7). This approach not only allows us to discriminate *in vivo* the spectro-temporal features of PSII–LHCII, PSI–LHCI(–LHCII) and uncoupled LHCII observed earlier in wild-type (WT) [10], but it also allows us to elucidate the fate of the antennae of the absent photosystem. Moreover, under varying environmental conditions some remodeling of the photosynthetic apparatus can take place which aims to sustain the optimal use of excitation energy and this change will also affect the EET. We therefore extended the present characterization of EET in the mutants by inducing in the cells one of such regulatory processes, the so-called state transitions (ST). This process is believed to maintain optimal excitation energy partitioning between PSI and PSII [11,12]. In *C.r.* it was proposed to play a role in photoprotection [13] and to maintain the physiological ATP/NADPH ratio [14], although the latter role was recently questioned [15]. State transitions are realized by LHCII complexes, which in state 1 (S1) transfer excitation energy mainly to PSII and upon transition to state 2 (S2) detach from PSII and at least part of them attaches to PSI. In *C.r.* the fraction of LHCII antennae which upon detachment from PSII effectively increases the absorption cross-section of PSI was initially suggested to account for 80% of the LHCII population [7], while recent reports indicate that it is far lower [10,16,17]. Upon mild isolation methods, PSI–LHCI– LHCII complexes were obtained

containing two LHCII trimers and one Lhcb monomer [18] or slightly smaller [19]. One of the steps in the cascade triggering the switch of LHCII complexes from PSII to PSI is an increase in the reduction of the plastoquinone (PQ) pool [20]. This rise results in the phosphorylation of LHCII which is supposed to increase its affinity towards PSI. In higher plants the reduction of the PQ pool can be achieved by illumination with light that preferentially excites PSII. In *C.r.* however, often another way of ST induction is applied, namely the cells are either incubated in the dark in aerobic conditions to keep the PQ pool oxidized (S1), or in the dark under anoxia to reduce the PQ pool (S2) [21–23]. In the present work we used the latter method to induce S1 and S2 in *C.r.* WT and mutants lacking the PSI core (M18 and F15) or the PSII core (FUD7). In the previous studies it was shown that both in the PSI-deficient mutants (C3 and M18) and in the PSII-deficient mutants (FUD7 and F34) LHCII is phosphorylated under anoxia in the dark [7,24,25].

In the present study we first describe excitation energy kinetics in the photosynthetic apparatus of *C.r.* strains deficient in either the PSI core or the PSII core (mutants F15, M18 and FUD7). Next, the change in excitation energy kinetics as a result of redistribution of the antenna complexes upon conditions mimicking state transitions is studied in the same strains. To that end the time-resolved fluorescence at 77 K measured in these mutants by means of streak camera was analyzed globally resulting in decay-associated spectra (DAS) of the fluorescence transients. Taking advantage of the reduced complexity of the photosynthetic apparatus in the mutants we confirm previous assignment of all features of the DAS measured in WT *C.r.* to specific excitation energy kinetics. Additionally, EET from PSII–LHCII and/or LHCII towards Lhca and fluorescence decay from Lhca, both not observed in WT, are characterized in the PSI-deficient mutants. We furthermore note that in one of the studied mutants deficient in the PSI core the trapping on PSII substantially decreases upon S1 → S2 transition. In the absence of the PSII core some LHCII complexes are uncoupled (quenched and unquenched form) and some other transfer energy to PSI. Transition to S2 leads to a stronger quenching of the former fraction and to an increased trapping by PSI.

Materials and methods

Strains, growth conditions and biochemical characterization Mutants F15 (cc-4138), M18 (cc-1051) and FUD7 (cc-4147) were purchased from the Chlamydomonas Resource Center (University of Minnesota). The direct effect of mutations introduced in F15 and in M18 is the lack of respectively PsaB and PsaA protein [26,27], while FUD7 is devoid of the D1 protein [21]. As a reference, *C.r.* WT strain 137c, a kind gift of Prof. Jean-David Rochaix, was used in the present work. The *C.r.* WT and mutant strains were grown in TAP medium [28] at 25

°C under low light conditions (<5 µE) on an incubator shaker (Minitron, INFORS HT). When the samples were taken for fluorescence measurements the cell number in the cultures was ≈4 × 10^6/ml.

The chlorophyll concentration was determined as described previously [29]. The values are averages ± standard deviation of three measurements. For the measurements the cells were concentrated to OD_{800nm} ≤ 2.

Total protein extraction was performed as described previously [30] and immunoblot analyses were performed as described in [31]. For primary antibodies, dilutions in PBS-T containing 5% nonfat milk were prepared as follows: D1 (1:5000), D2 (1:5000), PsaA (1:1000), CP43 (1:2500), CP26 (1:3000), CP29 (1:10,000), Lhcb2 (1:5000), Lhcbm5 (1:10,000), Lhca5 (1:1000). Except for the antibody for Lhca, which was a kind gift of Prof. Jean-David Rochaix, all other antibodies were purchased from Agrisera (Agrisera AB, Vännäs, Sweden). We note that antibody designated by Agrisera as Lhcbm5 recognizes most of the LhcbM proteins. LhcbM1 protein of *C.r.* is moreover specifically recognized by the Lhcb2 antibody [32]. To avoid deviation between different immunoblots, samples were compared only when loaded in the same gel.

For induction of state transitions *C.r.* cells were first pelleted (3 min, 4000 rpm) and then re-suspended in a fresh TAP medium previously either aerated or N2 bubbled for 1 h. The cells were kept in the dark and further respectively either aerated (S1 conditions) or N2 bubbled (S2 conditions) for 45 min [21,22]. After this time a Pasteur pipette was immersed in a sample and immediately quick-frozen in liquid nitrogen.

Spectroscopic measurements The full-spectrum time-resolved fluorescence was measured with a synchroscan streak camera setup described in detail by Gobets et al. [33]. The excitation pulses (≈100 fs) were generated using a tandem consisting of Vitesse Duo (Coherent, Santa Clara, California), regenerative amplifier RegA 9000 (Coherent, Santa Clara, California) and optical parametric amplifier (Coherent, Santa Clara, California). The samples frozen to 77 K in a Pasteur pipette were placed in a cold finger and excited at 400 nm with a repetition rate of 250 kHz and an energy per pulse of 1 nJ. The diameter of the excitation beam and the optical path length within the sample were both ≈1 mm. The fluorescence at the angle of 90° to the direction of the excitation beam was collimated and focused onto the input slit of spectrograph Chromex 250IS (Chromex, Albuquerque, New Mexico). An orange cut off filter OC11 was used here to block the scattered excitation light. Finally, the spectrally resolved emission was detected using a Hamamatsu C5680 synchroscan camera with a cooled Hamamatsu Digital Camera C10600-10B (ORCA-R2) (Hamamatsu Photonics,

Hamamatsu, Japan). The time window for acquisition was ≈1.5 ns (time range 4) resulting in the full-width at half maximum of the time response of ≈22 ps. The spectral window spanned 550–820 nm with a wavelength resolution of ≈4 nm. Per sample a sequence of sixty images of 10 s exposure time each was collected. Using the Hamamatsu High Performance Digital Temporal Analyzer (HPD-TA) 8.2.0., each sequence was averaged, background subtracted and corrected for the wavelength-dependent sensitivity of the detector (shading correction). Wavelength calibration was done by means of an argon lamp.

Global analysis [34] of the time-resolved fluorescence measured in the intact *C.r.* cells was performed using Glotaran ([35]; version 1.3). Global analysis means that at all recorded wavelengths (λ) simultaneously, the fluorescence decay is fitted with the sum of n parallel exponential decays (components) with rate constants $k_i = \tau_i^{-1}$, convolved with the instrument response function (IRF), taking into account dispersion. The fitted amplitude parameters for each component per wavelength constitute the so-called decay-associated spectra (DAS). The fitted fluorescence decay Ψ(t, λ) is thus described by the following equation:

$$\Psi(t,\lambda) = \sum_{i=1}^{n} [\exp(-k_i t) \otimes IRF(t)] DAS_i(\lambda).$$

This analysis was done either in the full spectral range of 640–760 nm to account for the kinetics of the whole photosynthetic apparatus or in wavelength ranges dominated by emission of antennae: Lhca kinetics was studied in F15 and M18 at 710–730 nm while LHCII kinetics was investigated in FUD7 at 670–683 nm. For each strain the DAS of S1 and of S2 were normalized using the estimated scaling number per dataset. This number is based on the total integrated area under the IRF and was obtained upon global analysis with linked rates of S1 and S2 datasets. We also checked that normalization based on the area under the spectrum at time zero (first Evolution-Associated Spectrum; [36]) delivers nearly the same results so that the present conclusions remain valid. The steady-state fluorescence spectra were reconstructed from globally analyzed time-resolved fluorescence by taking the sum of the DAS multiplied by their respective lifetimes, according to the following equation:

$$I(\lambda) = \Sigma DAS_i(\lambda)\tau_i .$$

The average lifetime of a decay dominated by LHCII emission, obtained upon global analysis of spectral range 670–683 nm in FUD7, was calculated according to the following equation:

$$\tau_{av} = \Sigma_{i=1}^{n} [\tau_i A_i] / \Sigma_{i=1}^{n} [A_i]$$

where A_i is the amplitude of the *i*th component at 681 nm.

Results

Protein composition of the photosynthetic apparatus in *C.r.* deficient in the PSI core or the PSII core

Previous biochemical characterization of *C.r.* mutants with impaired PSII showed that the lack of the D1 (PsbA) protein in FUD7 results in the absence of D2 (PsbD) and in a decrease of CP43 and CP47 when compared to WT [37]. Our results from immunoblot analysis on the full protein extract from FUD7 confirm the absence of D1 and D2 in this mutant while a small amount of CP43 and the components of PSI (PsaA, PsaD) as well as the antenna complexes of both photosystems (Lhca5, LhcbM5, LHCII) are present in the cells (Figure 3.10).

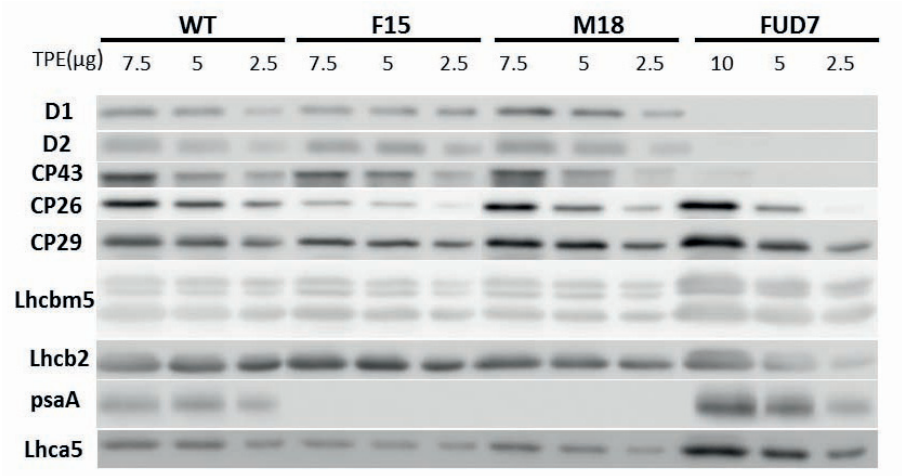

Figure 3.10 Immunoblot analysis of photosynthetic proteins in *C.r.* WT and the mutants F15, M18 and FUD7. In each blot, three sample (TPE: total protein extract) dilutions were loaded for each strain in order to prevent saturation. The three dilutions are in linear range. All strains were analyzed simultaneously on the same blot for each antibody. Note that the antibodies are named according to Agrisera specification, but Lhcbm5 is non-specific and recognized all there bands containing LhcbM proteins, while Lhcb2, rised against a peptide contained in Lhcb2 of plants, recognized specifically LhcbM1 of *C.r.* The latter feature is expected since LhcbM1 is the only LhcbM that contains this specific peptide.

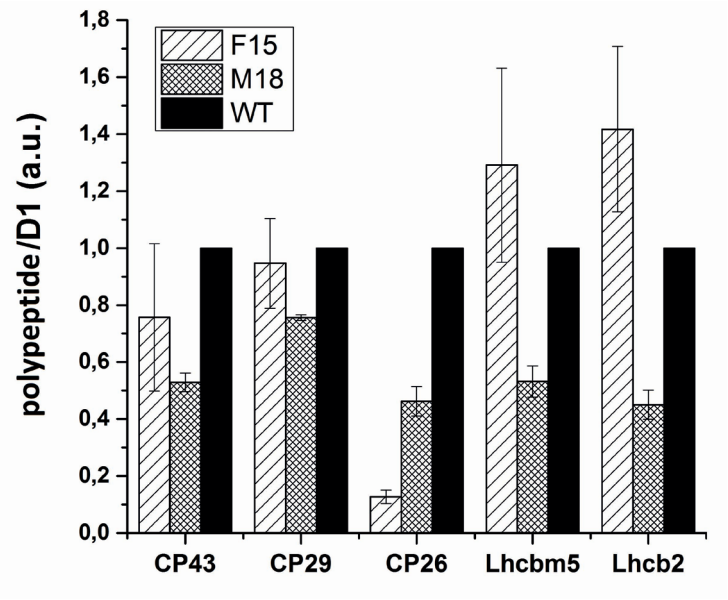

Figure 3.11 Ratio of inner and outer antenna proteins to the PSII core (D1 protein) based on the immunoblot analysis (Figure 3.10). The values obtained for WT were normalized to 1 and then the values obtained for the mutants F15 and M18 were converted accordingly. *a.u.*, arbitrary units.

The M18 mutant was shown to lack the PsaA protein [26], which is confirmed by our immunoblot analysis (Figure 3.10). It was moreover demonstrated that in the absence of PsaA, PsaB does not accumulate [38–40]. A similar effect is possibly responsible for the absence of the PsaA protein in F15, which has been characterized as a PsaB mutant. The antenna complexes of both photosystems are present in both these mutants. However, the relative amount of the individual antenna differs as F15 shows a strong reduction in CP26 (Figure 3.10, Figure 3.11). In M18 the amount of LhcbM relative to the PSII core subunits is lower than in WT (Figure 3.11), suggesting that the mutant has a smaller antenna size. This is in agreement with a previous study showing that the LhcbM genes in M18 appear to be downregulated when compared to WT [41]. The comparison of the pigment content of the cells leads to the same conclusions. The Chl *a/b* ratio of M18 is 2.3 while that of F15 is 1.9 (Table 3.3).

Table 3.3 Pigment composition in *C.r.* WT and the mutants F15, M18 and FUD7.

	Chl a (µg/ml)	Chl b (µg/ml)	Chl a+b (µg/ml)	Chl a/b
WT	4.85 ± 0.15	1.99 ± 0.08	6.85 ± 0.23	2.43 ± 0.025
F15	2.77 ± 0.03	1.46 ± 0.02	4.23 ± 0.02	1.89 ± 0.04
M18	2.20 ± 0.12	0.97 ± 0.06	3.17 ± 0.18	2.27 ± 0.03
FUD7	3.42 ± 0.19	1.3 ± 0.076	4.72 ± 0.26	2.63 ± 0.05

For other PSI-deficient strains an average value of 2.0 has been reported before [8]. Considering that the LhcbMs are the only complexes of the thylakoid membrane of *C.r.* with Chl *a/b* ratio below 1.9, and the PSII core is the only complex in these mutants with a Chl *a/b* clearly higher than 2.3, we can conclude that the ratio LhcbM/PSII core is higher in F15 than in M18.

77 K steady-state fluorescence emission

In Figure 3.12 we present 77 K steady-state fluorescence emission spectra of the WT and mutant cells incubated in S1 (black lines) or in S2 conditions (red lines). The spectra were derived from the time-resolved fluorescence measurements, as described in Materials and Methods. In the WT, the transition from S1 to S2 leads to a characteristic increase from 0.88 to 1.28 of the ratio of the PSI-dominated peak (F713) to the PSII-dominated peak (F685). As explained in our previous report [10], the latter band arises however not only from PSII (the well-known F685 emission band, the intensity of which decreases from S1 to S2), but also from X-685, an emission band attributed to quenched LHCII aggregates that occur almost exclusively in S2.

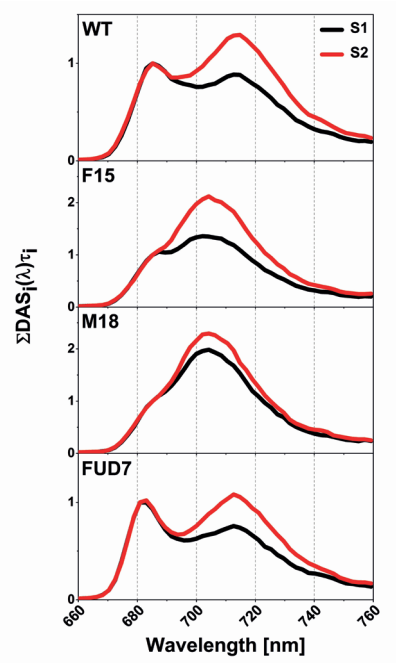

Figure 3.12 77 K fluorescence spectra reconstructed from globally analyzed time-resolved fluorescence measured in *C.r.* WT and mutants F15, M18 and FUD7 upon incubation in S1 conditions (black) or in S2 conditions (red). The spectra were normalized to 1 at 685 nm for WT, F15 and M18 and at 681 nm for FUD7. The samples were excited at 400 nm.

In the mutants lacking PSI (F15 and M18), the band F685 is observed at the same position as in the WT cells, confirming the presence of PSII (Figure 3.12). However, the emission spectra of these mutants clearly lack the fluorescence band F713, and instead show a broad band with a maximum at ≈704 nm (F704). A similar fluorescence spectrum was reported before for another PSI-deficient mutant Fl5 [42,43]. The biochemical analyses have indicated that the PSI core complex is absent in both mutants while the Lhca proteins are still present. The F704 band can be therefore attributed to Lhcas, which in various PSI-deficient cells or upon isolation emit at ≈707 nm at 77 K [43–48]. Upon the S1 → S2 transition, the F704/F685 ratio increases substantially from 1.35 to 2.12 in F15 and from 1.98 to 2.29 in M18, indicating that like in WT also in the cells without PSI, changes occur in the organization of the photosynthetic apparatus, though in these mutants the LHCII complexes cannot bind to PSI. The changes are more pronounced in F15 than in M18, possibly due to different LHCII amounts in these two strains, as indicated in above.

In the mutant deficient in PSII (the D1-minus mutant FUD7), the 77 K fluorescence spectra show a blue-shifted band peaking at 681 nm (F681) as well as the PSI band F713 observed

in WT (Figure 3.12). Similar spectra were observed before in other PSII deficient mutants, Fl39 [42,43] and F34 [25]. The typical F685 emission of PSII is not expected in this mutant and the emission at ≈680 nm can be attributed to LHCII [45,46], minor PSII antenna proteins [49,50] and CP43 not connected to a PSII reaction center [51]. Finally, the ratio of the two distinctive peaks F713/F681 in FUD7 increases upon the S1 → S2 transition from 0.76 to 1.08 suggesting that also in this mutant the organization of the photosynthetic apparatus changes upon applying S1 or S2 conditions.

The steady-state fluorescence measurements indicate that even in the absence of the PSI core or the PSII core, the remaining photosynthetic complexes still rearrange upon ST and this invariably leads to an increased intensity in S2 of the PSI/Lhca band relatively to the PSII/ LHCII band.

77 K time-resolved fluorescence emission: general characteristics of *C.r.* deficient in the PSI core or the PSII core

To understand the origin of the changes in the low-temperature fluorescence spectra, and to get information on the energy transfer processes in the *C.r.* mutant cells incubated under S1 or S2 conditions, we analyzed globally the time-resolved fluorescence (raw data are presented in the Supplementary Information, Figure S3.1). The complete spectrum (640–760 nm) of each dataset was thus fitted using four components. Adding a fifth component, as was done in our previous study on *C.r.* WT [10], did not improve the fit. The shortest component used in the previous study is absent here. This is presumably caused by the fact that in the present work the datasets were collected only in the longest (1.5 ns) time-window, thus the fastest (<10 ps) kinetics could not be resolved. Figure 3.13 shows the resulting decay-associated spectra (DAS) from WT and mutant cells incubated in S1 (black lines) or in S2 conditions (red lines). Note that we analyzed the kinetics of two PSI-deficient mutants, F15 and M18, both independently (open squares) and together with rates linked between the two strains (solid lines). Spectra at time zero are depicted in Figure S3.2. A comparison of the relative intensities of different DAS is shown in Figure S3.3.

Additionally, we analyzed globally the wavelength range 710–730nm in F15 and in M18 as well as 670–683 nm in FUD7. The former wavelength window is dominated by Lhca emission, while in the latter mainly LHCII emission is expected to contribute. The fitting of the narrow wavelength window in FUD7 requires four components (Table S3.1) similar to the full-spectrum fit, indicating that even EET kinetics dominated by LHCII complexes is still rather complicated. On the other hand, the Lhca-dominated emission in the PSI-deficient mutants is satisfactorily fitted with only two components (Table S3.1). The fluorescence

decays at ≈681 nm in case of FUD7 and at 715 nm in case of F15 and M18, together with their fits resulting from the global analysis are presented in Figure S3.4.

In all studied strains, the main lifetimes resulting from the global analysis of the full spectra are 20–30 ps, 100–135 ps, 400–500 ps and 2–3 ns. In the following, we first describe the possible origin of these lifetimes in each strain and subsequently we discuss the changes occurring upon the S1 → S2 transition.

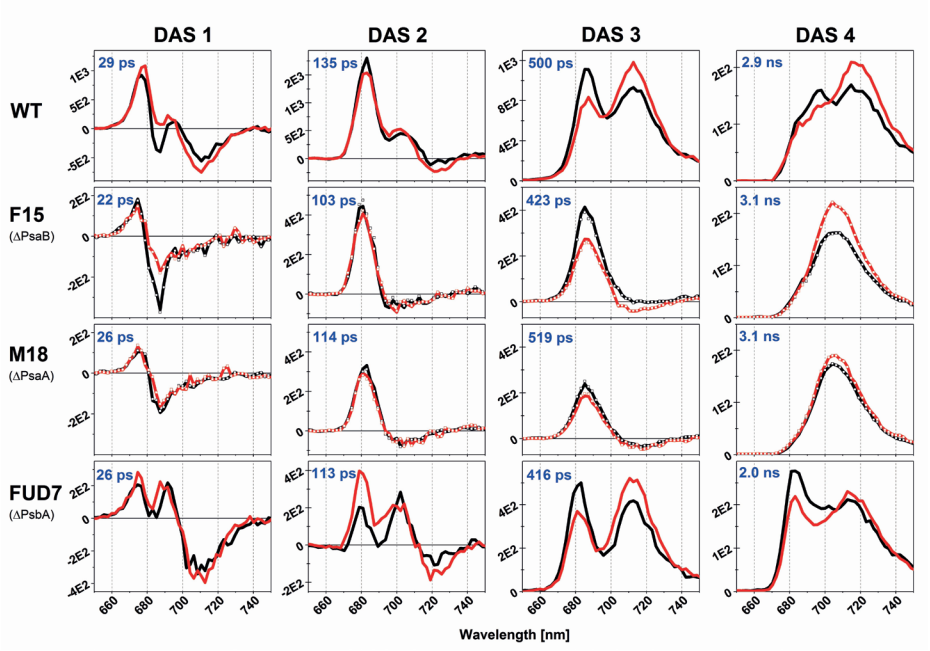

Figure 3.13 Decay-associated spectra (DAS) resulting from global analysis of 77 K time-resolved fluorescence measured in *C.r.* WT and mutants F15, M18 and FUD7 upon incubation in S1 conditions (black) or in S2 conditions (red). Spectra obtained for different states were normalized using a scaling number (for details, see Materials and Methods). PSI-deficient strains (F15 and M18) were analyzed independently (open squares) or with rates linked between both mutants (solid lines).

The 20–30 ps DAS

In WT, the DAS characterized by a lifetime of almost 30 ps shows a positive band at ≈675 nm and negative bands near 687 and 711 nm (Figure 3.13). Spectra with similar positive and negative peak positions were observed earlier in *C.r.* WT and in thylakoid membranes and PSII particles from spinach [10,52,53]. In these studies, the 675(+)/687(–) feature was attributed to EET from light-harvesting complexes to PSII whereas EET from bulk antennae to PSI was indicated as the origin of the 675(+)/>711(–) feature.

In both mutants lacking the PSI core (F15 and M18), the negative peak at 711 nm is missing completely. These spectra only show a positive peak at 675 nm and a negative peak at 687 nm. Hence, in the PSI-deficient mutants the EET from LHCII to the PSII core seems unaffected, while as expected energy transfer to PSI is absent.

In the mutant deficient in the PSII core (FUD7) the positive peak at 675 nm and the negative feature at 711 nm are clearly present, suggesting that excitation energy transfer from bulk antennae to PSI occurs just as in WT. However, additionally a negative peak at ≈685 nm appears, which can be explained by energy transfer from LHCII to complexes that are expected to emit around 685 nm, like remaining CP43 [51], and/or LHCII aggregates [54]. A positive peak at ≈691 nm followed by a negative feature at 711 nm depicts a downhill EET within the PSI–Lhca complexes [52].

The 100–135 ps DAS

Also in the second DAS, the spectral features of both PSI-deficient mutants F15 and M18 are simpler than those of the WT and of the PSII-deficient cells FUD7 (Figure 3.13). The second DAS of F15 and M18 have a clear positive peak at 681 nm which is followed by a zero-crossing at ≈692 nm to finally form a rather shallow but clear negative band at ≈702 nm. Except for the latter feature, this spectrum is very similar to that occurring with a lifetime of 132 ps in PSII membranes from spinach measured at 77 K [52]. Thus, the large positive amplitude suggests that excitations are trapped by PSII on this timescale, whereas the small negative band above 690 nm in F15 and M18 indicates the presence of some EET towards Lhca proteins that are present in these mutants but not in the PSII membranes.

A clear positive peak at ≈682 nm in the second DAS of WT can also in part be attributed to trapping on PSII, in agreement with our previous results from target analysis where nearly 60% of trapping on PSII occurred on the timescale of ≈170 ps [10]. In addition, there are positive and negative peaks at 703 and 722 nm, respectively, indicating EET from Lhca to PSI. In the PSII-deficient mutant FUD7, the up-and-down feature at 703 and 722 nm is clearly visible, while, relative to the positive band above 700 nm, the positive peak at 682 nm is much smaller than in WT, in agreement with the absence of the PSII core. In the mutant, the 682-nm band is probably dominated by fluorescence decay from Lhcb proteins. CP43 might also emit here, however its amount is very small relative to the Lhcb proteins (Figure 3.10). The relatively short lifetime of this decay indicates that the Lhcb complexes are quenched or transfer energy towards PSI. The negative feature at ≈689 nm in FUD7 is most probably also due to energy transfer to aggregated LHCII as discussed above for the ≈685-nm peak in DAS 1 of FUD7. Also CP43 can accept the excitation energy from LHCII [55], but this core antenna contributes only very little to emission at ≈689 nm [51].

The 400–500 ps DAS

Similarly to the first and second DAS, the spectral features of the 500-ps decay are simpler in the PSI-deficient mutants than in WT or in the PSII-deficient mutant (Figure 3.13). In F15 and M18, the spectrum of the third DAS shows a strong positive feature peaking at 685 nm and a zero or slightly negative amplitude around 715 nm. In PSII membranes measured at 77 K, the DAS with a lifetime of 500 ps peaking at 685 nm was observed [52] and attributed to the F685 emission band of PSII. However, the spectrum of this DAS in PSII membranes remains positive towards longer wavelengths resembling that of a chlorophyll absorption spectrum. The zero or negative amplitude at ≈715 nm in F15 and M18 suggests fluorescence rise, and because of the absence of PSI, it means that further energy equilibration towards the red-most forms of Lhca takes place on this timescale in the mutants.

Global analysis of the fluorescence emission dominated by Lhca in F15 and M18 (710–730 nm) delivers only one component with a negative amplitude, thus indicating excitation energy transfer to Lhcas (Table S3.1). The manifestation of this EET on two time scales in the full-spectrum analysis is possibly due to its lifetime of <220 ps, hence intermediate between the lifetimes characterizing the second (100– 135 ps) and the third (400–500 ps) DAS in the full-spectrum analysis.

In the WT cells the third DAS is positive at all wavelengths with peaks at 685 and 712 nm. The former band can be attributed to the F685 emission of PSII and some contribution of free LHCII (X-685 feature), while the emission at 712 nm originates from the red chlorophylls of PSI and trapping on PSI in agreement with previous results [10].

Trapping on PSI, visible as a positive band with a maximum at ≈713 nm occurs also in the PSII-deficient mutant FUD7, but in this case this band is accompanied by a strong peak at 681 nm. We suggest that this blue emission originates from the major peripheral antennae LHCII, which transfer energy to PSI and/or are present in a quenched form with a lifetime of ≈0.5 ns [16,56–58]. Also free CP43 can possibly contribute to this band, though the low amount of this protein when compared to LHCII excludes a major input from this core antenna.

The 2–3 ns DAS

All DAS characterized by the longest lifetime of 2–3 ns are positive, indicating decay of fluorescence (Figure 3.13). In WT, two maxima are observed at ≈713 and ≈695 nm, which are attributed to F713 of PSI and F695 of PSII, respectively.

In both PSI-deficient mutants the F713 emission is absent and instead a strong band peaking at 704 nm is observed that can be attributed to Lhca [43,45–48]. The absence of the 680-nm

feature in the F15 and M18 mutants indicates that all LHCII complexes are functionally attached and transfer energy to PSII or Lhca, or both or they are quenched. The 695-nm emission is expected in these cells as well, but most likely it is hidden under the strong Lhca signal at 704 nm.

In the PSII-deficient mutant the F713 band of PSI is obvious, but here also a second peak at 683 nm is observed, which most likely originates from the decay of major and minor light-harvesting complexes and CP43. The rather shallow valley between the 683- and the 712-nm band can possibly be caused by LHCII in an aggregated form. Upon isolation such LHCII aggregates have been shown to fluoresce at 695– 700 nm [59].

77 K time-resolved fluorescence emission: state transitions in *C.r.* deficient in the PSI core or in the PSII core

Even though the fluorescence emission has been measured in the mutants deficient in the PSI core or the PSII core incubated under S1 or S2 conditions [42,43], to our best knowledge the characterization of EET based on time-resolved full-spectrum fluorescence was not reported before. We want to stress that time-resolved fluorescence provides information about lifetimes and amplitudes separately. This allows us for example to directly discriminate between quenching and state transition. This information cannot be obtained by steady-state techniques.

In our study, we induced S1 conditions by bubbling the cells with air in the dark for 45 min, while anoxia obtained upon bubbling the cells with N2 in the dark for 45 min posed S2 conditions [21,22]. In WT cells, these conditions lead to oxidation and reduction of the plastoquinone pool, respectively. Transition from S2 to S1 in the mutants F15 and FUD7 is presented in Figure S3.5. The first DAS of WT cells in S1 (29 ps kinetics, black line), has a more pronounced negative peak at 686 nm than in S2 (red line), whereas the negative peak at 711 nm is more pronounced in S2 compared to S1. This result is in agreement with our earlier observations [10]. A negative peak means growth of fluorescence, thus in S1 the excitations are transferred to PSII, causing the negative peak at 686 nm, while in S2 this transfer is strongly reduced as indicated by the absence of the negative feature at 686 nm. On the other hand, the negative peak at 711 nm increases indicating more transfer to PSI. The spectra observed in the third (500 ps) and the fourth (2.9 ns) DAS confirm this conclusion, because in S1 more fluorescence decay occurs at 685 nm (DAS 3) and 695 nm (DAS 4) representing PSII emission, whereas in S2 fluorescence decay dominates at 712 nm (DAS 3) and 717 nm (DAS 4) that represent PSI emission. In our previous study, target analysis showed that energy transfer from LHCII to PSII/PSI occurs with two main lifetimes (now

largely lumped in DAS 1) and that in S2 a part of the signal at 685 nm must be attributed to quenched (DAS 3) and unquenched (DAS 4) - emission from LHCII-only aggregates [10].

State transitions in PSI-deficient cells

Figure 3.13 shows that both PSI-deficient mutants reveal different fluorescence kinetics in S1 vs S2. The M18 mutant, which has a higher Chl *a/b* ratio (Table 3.3) and a lower polypeptide/D1 ratio (Figure 3.10 and Figure 3.11) than the F15 strain, shows also much smaller differences between both states than F15. The trend of state transitions change in both mutants is however similar.

The first DAS of F15 shows a more negative peak at 687 nm in S1 (black line) than in S2 (red line), similarly as it is observed in the WT cells (Figure 3.13). This means that EET from the peripheral antenna complexes (largely LHCII) to PSII is more pronounced in S1 than in S2. Hence, it is likely that in S2 structural changes occurred that suppressed the transfer of energy from a part of the peripheral antennae to PSII. There is no sign of LHCII characterized by the longest lifetime of 3 ns (DAS 4), therefore if there are uncoupled bulk antennae present, they must be in a quenched state. On the other hand, the first DAS of the M18 mutant remains largely constant between S1 vs S2, suggesting that in this strain the EET from peripheral antennae to PSII is little sensitive to state transitions.

The far-red part of the first, second and third DAS of F15 and M18 carry direct information on the EET towards Lhca. The transfer occurring faster than 135 ps appears to be ST-independent in both PSI-mutants. The EET towards Lhca occurring with ≈500 ps barely changes in the M18 mutant, while in the F15 strain it is more pronounced in S2 vs S1. This change in the latter mutant is moreover accompanied by a reduced intensity of the PSII decay in S2 compared to S1, which is in agreement with the reduced EET to PSII in the first component of F15. As expected, the third DAS of M18 in S1 vs S2 changes little in the PSII emission region.

The somewhat larger EET towards Lhca observed in the third component of F15 in S2 when compared to S1 points at a situation in which more free Lhca complexes are energetically connected to PSII-LHCII and/or LHCII in S2 and therefore receive more energy in this state, but only on a slow time scale (in 500 ps). The resulting increase of fluorescence decay arising from Lhca is observed in the fourth DAS of F15. Although it is expected that at 695 nm the amplitude of the fourth DAS is larger in S1 than in S2, this change is presumably not visible due to the overlap of this band with relatively strong Lhca fluorescence which is more pronounced in S2. The difference in amplitude between S1 and S2 is smaller at 695 nm than at longer wavelengths at which less PSII contribution is expected, therefore qualitatively

this interpretation seems justified. Finally, as anticipated from the limited changes observed in the first three DAS of M18 in S1 vs S2, the fourth DAS varies only a little in this mutant.

State transitions in PSII-deficient cells

The PSII-deficient mutant FUD7 exhibits significant differences between the fluorescence transients measured upon incubation under S1 vs S2 conditions (Figure 3.10). In the first DAS, both the positive signal at 675 nm and the negative signal at 710 nm are slightly stronger in S2 than in S1. In the second DAS the amplitude of the positive 680-nm peak increases substantially while between 710 and 740 nm it becomes more negative. These results suggest that EET from bulk antenna complexes to PSI occurring with the lifetimes of 26 and 113 ps is more pronounced in S2 than in S1. This means that in S2 a larger part of the antennae is energetically coupled with PSI. The fluorescence decay transients in the third DAS confirm this interpretation: the broad band peaking at ≈713 nm has larger amplitude in S2, whereas the emission from unconnected LHCII at ≈681 nm has larger amplitude in S1. In the fourth DAS however mainly the 683-nm peak decreases upon transition to S2, while PSI emission does not increase significantly. Together with the shortening of the average LHCII-dominated fluorescence decay lifetime from 645 ps in S1 to 484 ps in S2 (Table S3.1), these results suggest that upon the S1→S2 transition some LHCII complexes transfer energy to PSI while other LHCII antennae remain uncoupled and become quenched.

Discussion

Organization of the thylakoid membranes in *C.r.* deficient in the PSI core or the PSII core

The photosynthetic membranes are densely packed with pigment–protein complexes whose specific arrangement determines possible excitation energy transfer routes. In higher plants, PSII–LHCII complexes are mainly present in stacks of multiple discs (grana), while the interconnecting single discs (stroma lamellae) are occupied mostly by PSI–Lhca [60]. In *C.r.* however the membranes forma network of single discs or elongated, bifurcating and merging stacks of only a couple of discs [61,62], thus it is expected that the separation between the PSI- and PSII-rich areas is less pronounced here.

It has been shown that in the *C.r.* mutants lacking crucial parts of the photosynthetic apparatus, the arrangement of membranes can be different from that in WT [61]. Generally, PSII-deficient mutants seem to have rather unstacked thylakoid membranes, while large grana-like stacks are formed in mutants lacking PSI [63].

PSI-deficient mutants: F15 and M18

The absence of the PSI core in the mutants F15 and M18 results in a functional coupling of Lhca to PSII–LHCII and/or LHCII complexes (Figure 3.13). A similar observation has been made before for other PSI-deficient mutants [7,8]. In the F15 mutant we see that upon transition to S2 excitation energy transfer from PSII–LHCII and/or LHCII to Lhca increases. Such change is far smaller in the M18 cells. Our biochemical characterization of the two strains provides a possible explanation of this discrepancy. Both the Chl *a/b* ratio (Table 3.3) and the polypeptide/D1 ratio (Figure 3.10 and Figure 3.11) indicate that F15 has more bulk antennae when compared to the M18 cells. It has been shown, that state transitions are accompanied by rearrangement of the thylakoids (changes in stacking), both in higher plants [64,65] and in *C.r.* [66], as well as by disassembly of the PSII–LHCII megacomplexes into supercomplexes [66]. Moreover, various amounts of Lhcb can lead to a different arrangement of the photosynthetic complexes embedded in the membranes and of the membranes themselves [67–69]. Finally, a decreased amount of certain LhcbMs diminishes ST in *C.r.* [70,71]. All these observations strongly support our conclusion that the different magnitude of ST in F15 vs M18 originates from the distinct composition of the photosynthetic apparatus in these two strains. Although this is the most likely explanation, we cannot exclude that there are other unidentified mutations that either diminish state transition (in M18) or enhance it (in F15). Our results show that induction of ST in *C.r.* can lead to a rearrangement of the photosynthetic apparatus in the absence of the PSI core, however in light of the extensive changes and different content of peripheral antennae between the two PSI-deficient strains that we used in the present study, further work will be needed to understand exactly what is the extent of antenna reorganization upon ST in the mere absence of PSI cores. Independent of the state, the M18 strain shows EET kinetics similar to the one of the F15 cells in S2. This observation suggests that the arrangement of photosynthetic complexes and possibly membranes in the M18 cells resembles that of F15 under S2 conditions.

Finally, the change in EET from PSII–LHCII and/or LHCII complexes to Lhca observed in F15 upon S1→S2 transition affects component characterized by a relatively long lifetime (423 ps).We suggest therefore that these Lhcas are rather loosely connected to the PSII–LHCII and/or LHCII complexes.

PSII-deficient mutant FUD7

Thylakoid membranes of PSII-deficient mutants show a reduced stacking when compared to WT [61,63]. A possible consequence of such arrangement is a relatively high mobility and intermixing of the remaining pigment–protein complexes. In the PSII-deficient mutant F34, it was shown that upon reduction of the PQ pool, LHCII was phosphorylated and as a

result the fluorescence quantum yield decreased [25,72]. Similarly, fluorescence kinetics measured on FUD7 indicated reduction of the PQ pool under anoxia in the dark [24], which are the conditions used in the present study. Our results show that in FUD7 independently of the state some of the LHCII complexes are uncoupled and some transfer excitation energy towards PSI. By means of the full-spectrum time-resolved fluorescence we can distinguish these two phenomena and we observe that upon S1 → S2 transition some of the uncoupled LHCII complexes become (more) quenched as well as the EET from LHCII complexes towards PSI increases. Both changes result also in shortening of the average lifetime of the fluorescence decay dominated by LHCII emission (Table S3.1, Figure S3.4).

Conclusions

In this work we studied excitation energy transfer in the photosynthetic apparatus of intact cells of *C.r.* deficient in the PSI core or the PSII core. The PSI-deficient mutants, F15 and M18, show kinetics similar to that of the PSII membranes from spinach [52] and the differences are well explained by the presence of Lhcas solely in the former ones. Moreover, we observe that at 77 K these Lhcas can act as traps of excitation energy from PSII–LHCII and/or LHCII. Upon transition from state 1 to state 2 an increase of this EET and a decrease of trapping by PSII are observed in the F15 mutant, while in the M18 mutant these changes are limited.

In the PSII-deficient mutant, FUD7, some of the LHCII complexes transfer excitation energy towards PSI while others are uncoupled. Upon S1 → S2 transition both more EET towards PSI and an increased quenching of the free LHCII complexes are observed. The presence of LHCII populations in a different quenching state is in agreement with recent results on LHCII-only membranes of *C.r.* [58].

Using mutants of *C.r.* we show that detachment of LHCII from PSII and association of LHCII with PSI upon state transitions pose two independent processes. This result is in line with the previous observations that in *C.r.* wild-type part of LHCII is disconnecting from PSII without associating with PSI [10,16,17]. Moreover, these observations support an earlier suggestion that state transitions in *C.r.* have a protective role occurring as a temporal solution during the buildup of nonphotochemical quenching [13].

Spectroscopic studies on intact cells of *C.r.* reveal the functional interaction between different photosynthetic pigment–protein complexes and how these interactions change upon state transitions [10,16,17]. These results point to structural re-arrangements of the complexes. A combination of this knowledge with structural information, derived e.g.

from a freeze-fracture study, could finally provide the full picture of the remodeling of the photosynthetic apparatus upon state transitions in this green alga.

References

1. Dekker, J. P. & Boekema, E. J. Supramolecular organization of thylakoid membrane proteins in green plants. *Biochim. Biophys. Acta - Bioenerg.* **1706,** 12–39 (2005).
2. Croce, R. & van Amerongen, H. Natural strategies for photosynthetic light harvesting. *Nat. Chem. Biol.* **10,** 492–501 (2014).
3. Pan, X., Liu, Z., Li, M. & Chang, W. Architecture and function of plant light-harvesting complexes II. *Curr. Opin. Struct. Biol.* **23,** 515–525 (2013).
4. Natali, A. & Croce, R. Characterization of the Major Light-Harvesting Complexes (LHCBM) of the Green Alga Chlamydomonas reinhardtii. *PLoS One* **10,** (2015).
5. Mozzo, M., Mantelli, M., Passarini, F., Caffarri, S., Croce, R. & Bassi, R. Functional analysis of Photosystem I light-harvesting complexes (Lhca) gene products of Chlamydomonas reinhardtii. *Biochim. Biophys. Acta - Bioenerg.* **1797,** 212–221 (2010).
6. Teramoto, H., Ono, T. & Minagawa, J. Identification of Lhcb Gene Family Encoding the Light-harvesting Chlorophyll-a/b Proteins of Photosystem II in Chlamydomonas reinhardtii. *Plant Cell Physiol.* **42,** 849–856 (2001).
7. Delosme, R., Olive, J. & Wollman, F.-A. Changes in light energy distribution upon state transitions: an in vivo photoacoustic study of the wild type and photosynthesis mutants from Chlamydomonas reinhardtii. *Biochim. Biophys. Acta - Bioenerg.* **1273,** 150–158 (1996).
8. Bennoun, P. & Jupin, H. Spectral properties of system I-deficient mutants of Chlamydomonas reinhardi. Possible occurrence of uphill energy transfer. *Biochim. Biophys. Acta - Bioenerg.* **440,** 122–130 (1976).
9. Blankenship, R. E. Molecular Mechanisms of Photosynthesis. (ed. Blankenship, R. E.) (Blackwell Science Ltd, 2002).
10. Wlodarczyk, L. M., Snellenburg, J. J., Ihalainen, J. A., van Grondelle, R., van Stokkum, I. H. M. & Dekker, J. P. Functional Rearrangement of the Light-Harvesting Antenna upon State Transitions in a Green Alga. *Biophys. J.* **108,** 261–271 (2015).
11. Murata, N. Control of excitation transfer in photosynthesis I. Light-induced change of chlorophyll a fluoresence in Porphyridium cruentum. *Biochim. Biophys. Acta - Bioenerg.* **172,** 242–251 (1969).
12. Bonaventura, C. & Myers, J. Fluorescence and oxygen evolution from Chlorella pyrenoidosa. *Biochim. Biophys. Acta - Bioenerg.* **189,** 366–383 (1969).
13. Allorent, G., Tokutsu, R., Roach, T., Peers, G., Cardol, P., Girard-Bascou, J., Seigneurin-Berny, D., Petroutsos, D., Kuntz, M., Breyton, C., Franck, F., Wollman, F.-A., Niyogi, K. K., Krieger-Liszkay, A., Minagawa, J. & Finazzi, G. A Dual Strategy to Cope with High Light in Chlamydomonas reinhardtii. *Plant Cell* **25,** 545–557 (2013).
14. Finazzi, G., Furia, A., Barbagallo, R. P. & Forti, G. State transitions, cyclic and linear electron transport and photophosphorylation in Chlamydomonas reinhardtii. *Biochim. Biophys. Acta - Bioenerg.* **1413,** 117–129 (1999).
15. Takahashi, H., Clowez, S., Wollman, F.-A., Vallon, O. & Rappaport, F. Cyclic electron flow is redox-controlled but independent of state transition. *Nat. Commun.* **4,** 1954 (2013).

16. Unlü, C., Drop, B., Croce, R. & van Amerongen, H. State transitions in Chlamydomonas reinhardtii strongly modulate the functional size of photosystem II but not of photosystem I. *Proc. Natl. Acad. Sci. U. S. A.* **111,** 3460–5 (2014).

17. Nagy, G., Ünnep, R., Zsiros, O., Tokutsu, R., Takizawa, K., Porcar, L., Moyet, L., Petroutsos, D., Garab, G., Finazzi, G. & Minagawa, J. Chloroplast remodeling during state transitions in *Chlamydomonas reinhardtii* as revealed by noninvasive techniques in vivo. *Proc. Natl. Acad. Sci.* **111,** 5042–5047 (2014).

18. Drop, B., Yadav K.N., S., Boekema, E. J. & Croce, R. Consequences of state transitions on the structural and functional organization of Photosystem I in the green alga *Chlamydomonas reinhardtii*. *Plant J.* **78,** 181–191 (2014).

19. Takahashi, H., Okamuro, A., Minagawa, J. & Takahashi, Y. Biochemical characterization of photosystem I-associated light-harvesting complexes i and II isolated from state 2 cells of chlamydomonas reinhardtii. *Plant Cell Physiol.* **55,** 1437–1449 (2014).

20. Allen, J. F., Bennett, J., Steinback, K. E. & Arntzen, C. J. Chloroplast protein phosphorylation couples plastoquinone redox state to distribution of excitation energy between photosystems. *Nature* **291,** 25–29 (1981).

21. Wollman, F.-A. & Lemaire, C. Studies on kinase-controlled state transitions in Photosystem II and b6f mutants from Chlamydomonas reinhardtii which lack quinone-binding proteins. *Biochim. Biophys. Acta - Bioenerg.* **933,** 85–94 (1988).

22. Bulté, L., Gans, P., Rebéillé, F. & Wollman, F.-A. ATP control on state transitions in vivo in Chlamydomonas reinhardtii. *Biochim. Biophys. Acta - Bioenerg.* **1020,** 72–80 (1990).

23. Finazzi, G., Barbagallo, R. P., Bergo, E., Barbato, R. & Forti, G. Photoinhibition of Chlamydomonas reinhardtii in State 1 and State 2. Damages to the photosynthetic apparatus under linear and cyclic electron flow. *J. Biol. Chem.* **276,** 22251–22257 (2001).

24. Bennoun, P., Spiererherz, M., Erickson, J., Girard-Bascoul, J., Pierre, Y., Delosme, M. & Rochaix, J.-D. Characterization of Photosystem-Ii Mutants of Chlamydomonas reinhardtii Lacking the Psba Gene. *Plant Mol. Biol.* **6,** 151–160 (1986).

25. Wollman, F. A. & Delepelaire, P. Correlation between changes in light energy distribution and changes in thylakoid membrane polypeptide phosphorylation in Chlamydomonas reinhardtii. *J. Cell Biol.* **98,** 1–7 (1984).

26. Girard, J., Chua, N. H., Bennoun, P., Schmidt, G. & Delosme, M. Studies on Mutants Deficient in the Photosystem-I Reaction Centers in Chlamydomonas reinhardtii. *Curr. Genet.* **2,** 215–221 (1980).

27. Stampacchia, O., Girard-Bascou, J., Zanasco, J. L., Zerges, W., Bennoun, P. & Rochaix, J.-D. A nuclear-encoded function essential for translation of the chloroplast psaB mRNA in Chlamydomonas. *Plant Cell* **9,** 773–782 (1997).

28. Gorman, D. S. & Levine, R. P. Cytochrome f and plastocyanin: their sequence in the photosynthetic electron transport chain of Chlamydomonas reinhardi. *Proc. Natl. Acad. Sci.* **54,** 1665–1669 (1965).

29. Croce, R., Canino, G., Ros, F. & Bassi, R. Chromophore organization in the higher-plant photosystem II antenna protein CP26. *Biochemistry* **41,** 7334–7343 (2002).

30. Ramundo, S., Rahire, M., Schaad, O. & Rochaix, J.-D. Repression of Essential Chloroplast Genes Reveals New Signaling Pathways and Regulatory Feedback Loops in Chlamydomonas. *Plant Cell* **25,** 167–186 (2013).

31. Dinc, E., Ramundo, S., Croce, R. & Rochaix, J.-D. Repressible chloroplast gene expression in Chlamydomonas: A new tool for the study of the photosynthetic apparatus. *Biochim. Biophys. Acta* **1837,** 1548–1552 (2013).

32. Drop, B., Webber-Birungi, M., Yadav, S. K. N., Filipowicz-Szymanska, A., Fusetti, F., Boekema, E. J. & Croce, R. Light-harvesting complex II (LHCII) and its supramolecular organization in Chlamydomonas reinhardtii. *Biochim. Biophys. Acta - Bioenerg.* **1837,** 63–72 (2014).

33. Gobets, B., Van Stokkum, I. H. M., Rögner, M., Kruip, J., Schlodder, E., Karapetyan, N. V., Dekker, J. P. & Van Grondelle, R. Time-resolved fluorescence emission measurements of photosystem I particles of various cyanobacteria: A unified compartmental model. *Biophys. J.* **81,** 407–424 (2001).

34. Van Stokkum, I. H. M., Larsen, D. S. & Van Grondelle, R. Global and target analysis of time-resolved spectra. *Biochim. Biophys. Acta - Bioenerg.* **1657,** 82–104 (2004).

35. Snellenburg, J. J., Laptenok, S. P., Seger, R., Mullen, K. M. & van Stokkum, I. H. M. Glotaran: a Java -based graphical user interface for the R-package TIMP. *J. Stat. Softw.* **49,** 1–23 (2012).

36. Van Stokkum, I. H. M., Van Oort, B., Van Mourik, F., Gobets, B. & Van Amerongen, H. (Sub)-Picosecond Spectral Evolution of Fluorescence Studied with a Synchroscan Streak-Camera System and Target Analysis. in *Biophys. Tech. Photosynth.* 223–240 (2008).

37. de Vitry, C., Olive, J., Drapier, D., Recouvreur, M. & Wollman, F.-A. Posttranslational events leading to the assembly of photosystem II protein complex: a study using photosynthesis mutants from Chlamydomonas reinhardtii. *J. Cell Biol.* **109,** 991–1006 (1989).

38. Goldschmidt-Clermont, M., Girard-Bascou, J., Choquet, Y. & Rochaix, J.-D. Trans-splicing mutants of Chlamydomonas reinhardtii. *MGG Mol. Gen. Genet.* **223,** 94305 (1990).

39. Girard-Bascou, J., Choquet, Y., Schneider, M., Delosme, M. & Dron, M. Characterization of a chloroplast mutation in the psaA2 gene of Chlamydomonas reinhardtii. *Curr. Genet.* **12,** 489–495 (1987).

40. Wostrikoff, K., Girard-Bascou, J., Wollman, F.-A. & Choquet, Y. Biogenesis of PSI involves a cascade of translational autoregulation in the chloroplast of Chlamydomonas. *EMBO J.* **23,** 2696–2705 (2004).

41. Balczun, C., Bunse, A., Nowrousian, M., Korbel, A., Glanz, S. & Kück, U. DNA macroarray and real-time PCR analysis of two nuclear photosystem I mutants from Chlamydomonas reinhardtii reveal downregulation of Lhcb genes but different regulation of Lhca genes. *Biochim. Biophys. Acta - Gene Struct. Expr.* **1732,** 62–68 (2005).

42. Maroc, J., Garnier, J. & Guyon, D. Chlorophyll—protein complexes related to photosystem I in Chlamydomonas reinhardtii. *J. Photochem. Photobiol. B Biol.* **4,** 97–109 (1989).

43. Garnier, J., Maroc, J. & Guyon, D. Low-temperature fluorescence emission spectra and chlorophyll-protein complexes in mutants of Chlamydomonas reinhardtii: Evidence for a new chlorophyll-a-protein complex related to Photosystem I. *Biochim. Biophys. Acta - Bioenerg.* **851,** 395–406 (1986).

44. Wollman, F.-A. & Bennoun, P. A new chlorophyll-protein complex related to Photosystem I in Chlamydomonas reinhardii. *Biochim. Biophys. Acta - Bioenerg.* **680,** 352–360 (1982).

45. Lebedev, N. N., Khatyrov, R. A., Ladygin, V. A. & Krasnovskii, A. A. Fluorescence excitation spectra and decay kinetics of light-harvesting complex in Chlamydomonas reinhardtii mutants. *Photosynthetica* **22,** 364–370 (1988).

46. Lin, S. & Knox, R. S. Studies of excitation energy transfer within the green alga Chlamydomonas reinhardtii and its mutants at 77 K. *Photosynth. Res.* **27,** 157–68 (1991).

47. Bassi, R., Su Yin Soen, Frank, G., Zuber, H. & Rochaix, J.-D. Characterization of chlorophyll a/b proteins of photosystem I from Chlamydomonas reinhardtii. *J. Biol. Chem.* **267,** 25714–25721 (1992).

48. Takahashi, Y., Yasui, T., Stauber, E. & Hipplers, M. Comparison of the Subunit Compositions of the PSI-LHCI Supercomplex and the LHCI in the Green Alga Chlamydomonas reinhardtii. *Biochemistry* 7816–7823 (2004).

49. Bassi, R. & Wollman, F.-A. The chlorophyll-a/b proteins of photosystem II in Chlamydomonas reinhardtii. *Planta* **183,** 423–433 (1991).

50. Pascal, A., Gradinaru, C., Wacker, U., Peterman, E., Calkoen, F., Irrgang, K. D., Horton, P., Renger, G., van Grondelle, R., Robert, B. & van Amerongen, H. Spectroscopic characterization of the spinach Lhcb4 protein (CP29), a minor light-harvesting complex of photosystem II. *Eur. J. Biochem.* **262,** 817–823 (1999).

51. Groot, M. L., Frese, R. N., de Weerd, F. L., Bromek, K., Pettersson, a, Peterman, E. J., van Stokkum, I. H., van Grondelle, R. & Dekker, J. P. Spectroscopic properties of the CP43 core antenna protein of photosystem II. *Biophys. J.* **77,** 3328–3340 (1999).

52. van der Weij-de Wit, C. D., Ihalainen, J. A., van Grondelle, R. & Dekker, J. P. Excitation energy transfer in native and unstacked thylakoid membranes studied by low temperature and ultrafast fluorescence spectroscopy. *Photosynth. Res.* **93,** 173–182 (2007).

53. Komura, M., Shibata, Y. & Itoh, S. A new fluorescence band F689 in photosystem II revealed by picosecond analysis at 4-77 K: Function of two terminal energy sinks F689 and F695 in PS II. *Biochim. Biophys. Acta - Bioenerg.* **1757,** 1657–1668 (2006).

54. Vasil'ev, S., Irrgang, K. D., Schrötter, T., Bergmann, A., Eichler, H. J. & Renger, G. Quenching of chlorophyll a fluorescence in the aggregates of LHCII: Steady state fluorescence and picosecond relaxation kinetics. *Biochemistry* **36,** 7503–7512 (1997).

55. Bassi, R., Høyer-Hansen, G., Barbato, R., Giacometti, G. M. & Simpson, D. J. Chlorophyll-proteins of the photosystem II antenna system. *J. Biol. Chem.* **262,** 13333–41 (1987).

56. Moya, I., Silvestri, M., Vallon, O., Cinque, G. & Bassi, R. Time-resolved fluorescence analysis of the photosystem II antenna proteins in detergent micelles and liposomes. *Biochemistry* **40,** 12552–12561 (2001).

57. van Oort, B., Alberts, M., De Bianchi, S., Dall'Osto, L., Bassi, R., Trinkunas, G., Croce, R. & van Amerongen, H. Effect of antenna-depletion in photosystem II on excitation energy transfer in Arabidopsis thaliana. *Biophys. J.* **98,** 922–931 (2010).

58. Tian, L., Dinc, E. & Croce, R. LHCII Populations in Different Quenching States Are Present in the Thylakoid Membranes in a Ratio that Depends on the Light Conditions. *J. Phys. Chem. Lett.* 2339–2344 (2015).

59. Mullineaux, C. W., Pascal, A. A., Horton, P. & Holzwarth, A. R. Excitation-Energy Quenching in Aggregates of the Lhc-Ii Chlorophyll-Protein Complex - a Laser-Induced Optoacoustic Study. *Biochim. Biophys. Acta* **1143,** 235–238 (1993).

60. Andersson, B. & Anderson, J. M. Lateral heterogeneity in the distribution of chlorophyll-protein complexes of the thylakoid membranes of spinach chloroplasts. *Biochim. Biophys. Acta - Bioenerg.* **593,** 427–440 (1980).

61. Goodenough, U. W. & Levine, R. P. Chloroplast Ultrastructure in Mutant Strains of Chlamydomonas reinhardi Lacking Components of the Photosynthetic Apparatus. *Plant Physiol.* **44,** 990–1000 (1969).

62. Engel, B. D., Schaffer, M., Cuellar, L. K., Villa, E., Plitzko, J. M. & Baumeister, W. Native architecture of the Chlamydomonas chloroplast revealed by in situ cryo-electron tomography. *eLife* **2015,** 1–29 (2015).

63. Harris, E. H. The Chlamydomonas Sourcebook: A Comprehensive Guide to Biology and Laboratory Use. (Academic Press, 1989).

64. Chuartzman, S. G., Nevo, R., Shimoni, E., Charuvi, D., Kiss, V., Ohad, I., Brumfeld, V. & Reich, Z. Thylakoid Membrane Remodeling during State Transitions in Arabidopsis. *Plant Cell* **20,** 1029–1039 (2008).

65. Rozak, P. R., Seiser, R. M., Wacholtz, W. F. & Wise, R. R. Rapid, reversible alterations in spinach thylakoid appression upon changes in light intensity. *Plant, Cell Environ.* **25,** 421–429 (2002).

66. Iwai, M., Takahashi, Y. & Minagawa, J. Molecular Remodeling of Photosystem II during State Transitions in Chlamydomonas reinhardtii. *Plant Cell* **20,** 2177–2189 (2008).

67. Burke, J. J., Steinback, K. E. & Arntzen, C. J. Analysis of the Light-harvesting Pigment-Protein Complex of Wild Type and a Chlorophyll-b-less Mutant of Barley. *PLANT Physiol.* **63,** 237–243 (1979).

68. Bassi, R., Hinz, U. & Barbato, R. The role of the light harvesting complex and photosystem II in thylakoid stacking in thechlorina-f2 barley mutant. *Carlsberg Res. Commun.* **50,** 347–367 (1985).

69. Kouřil, R., Wientjes, E., Bultema, J. B., Croce, R. & Boekema, E. J. High-light vs. low-light: Effect of light acclimation on photosystem II composition and organization in Arabidopsis thaliana. *Biochim. Biophys. Acta - Bioenerg.* **1827,** 411–419 (2013).

70. Ferrante, P., Ballottari, M., Bonente, G., Giuliano, G. & Bassi, R. LHCBM1 and LHCBM2/7 Polypeptides, Components of Major LHCII Complex, Have Distinct Functional Roles in Photosynthetic Antenna System of Chlamydomonas reinhardtii. *J. Biol. Chem.* **287,** 16276–16288 (2012).

71. Takahashi, H., Iwai, M., Takahashi, Y. & Minagawa, J. Identification of the mobile light-harvesting complex II polypeptides for state transitions in Chlamydomonas reinhardtii. *Proc. Natl. Acad. Sci.* **103,** 477–482 (2006).

72. Delepelaire, P. & Wollman, F.-A. Correlations between fluorescence and phosphorylation changes in thylakoid membranes of Chlamydomonas reinhardtii in vivo: A kinetic analysis. *Biochim. Biophys. Acta - Bioenerg.* **809,** 277–283 (1985).

Supporting Information

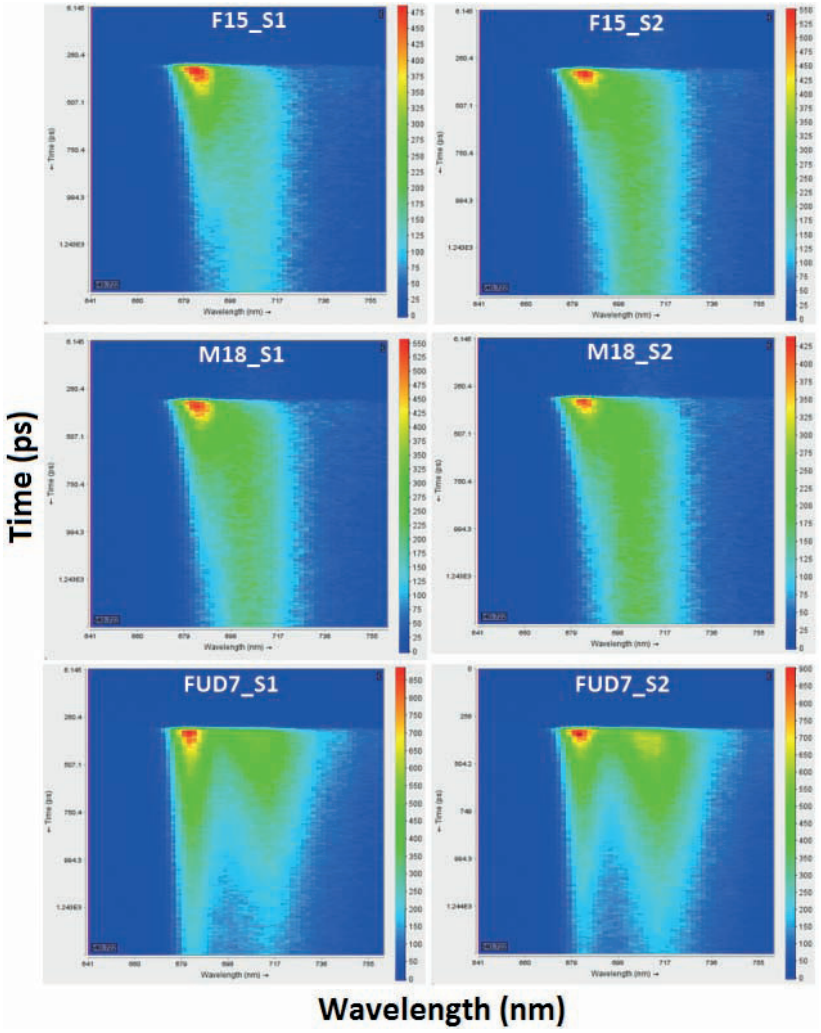

Figure S3.8 Full-spectrum fluorescence kinetics of *C.r.* WT and mutants F15, M18 and FUD7 measured at 77 K with streak camera. Fluorescence emission intensity is color-coded from zero (blue) to the highest value (red).

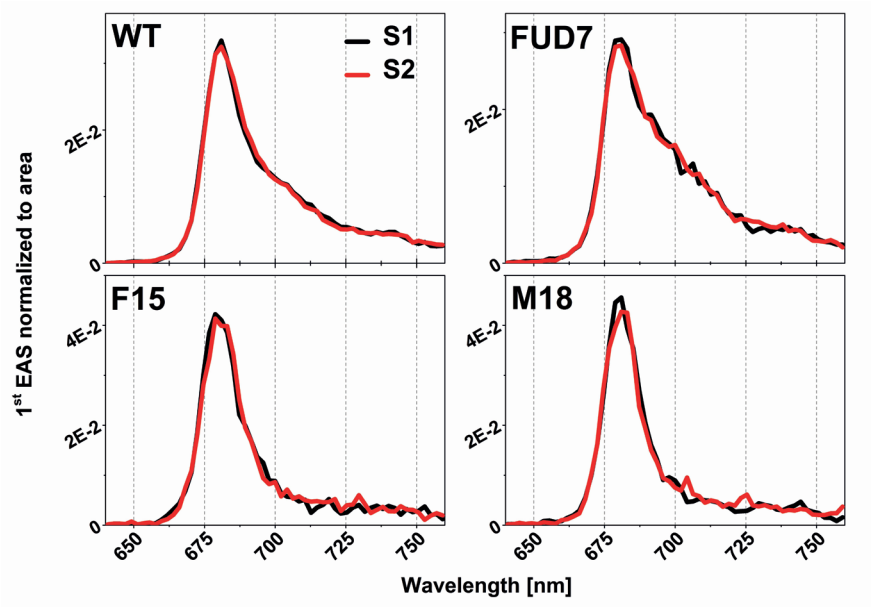

Figure S3.9 First EAS (Evolution-Associated Spectra) representing the spectra at time zero (deconvoluted and dispersion corrected) resulting from global analysis of 77 K time-resolved fluorescence measured in *C.r.* WT and mutants F15, M18 and FUD7 upon incubation in S1 conditions (black) or in S2 conditions (red). Each spectrum was normalized to the area under the spectrum.

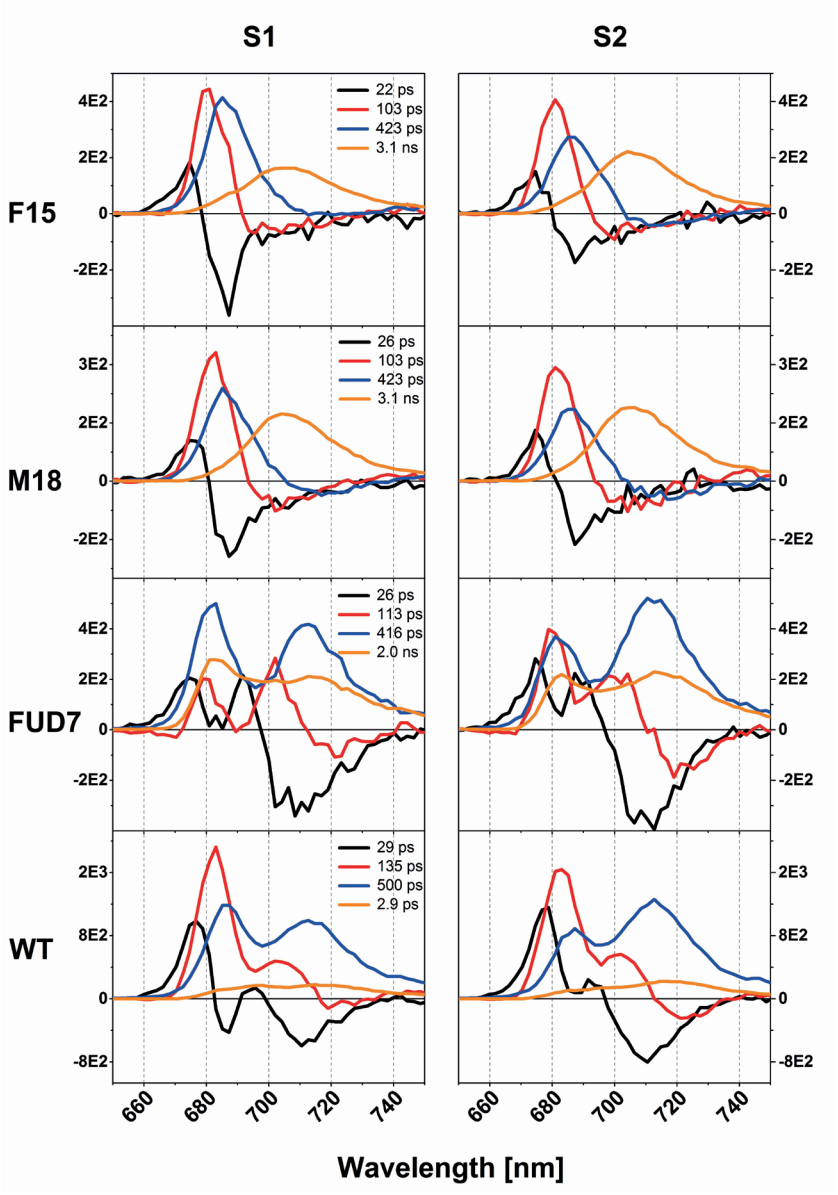

Figure S3.10 Decay-Associated Spectra (DAS) resulting from global analysis of 77 K time-resolved fluorescence measured in *C.r.* WT and mutants F15 , M18 and FUD7 upon incubation in S1 conditions (left panel) or in S2 conditions (right panel).

Table S3.1 Lifetimes (ps) obtained upon global fit in 670-683 nm for FUD7 and in 710-730 nm for F15 and M18. Amplitudes at 715 nm for F15 and M18 and at 681 nm for FUD7 are indicated.

		τ_1	A_1	τ_2	A_2	τ_3	A_3	τ_4	A_4	τ_{ave}
F15	S1	**60**	*-56*	**3104**	*104*	**-**	-	**-**	-	**-**
	S2	**164**	*-66*	**3384**	*159*	**-**	-	**-**	-	**-**
M18	S1	**218**	*-60*	**3176**	*159*	**-**	-	**-**	-	**-**
	S2	**185**	*-62*	**3467**	*132*	**-**	-	**-**	-	**-**
FUD7	S1	**27**	*138*	**172**	*271*	**463**	*289*	**1700**	*252*	**645**
	S2	**24**	*171*	**112**	*396*	**418**	*322*	**1920**	*172*	**484**

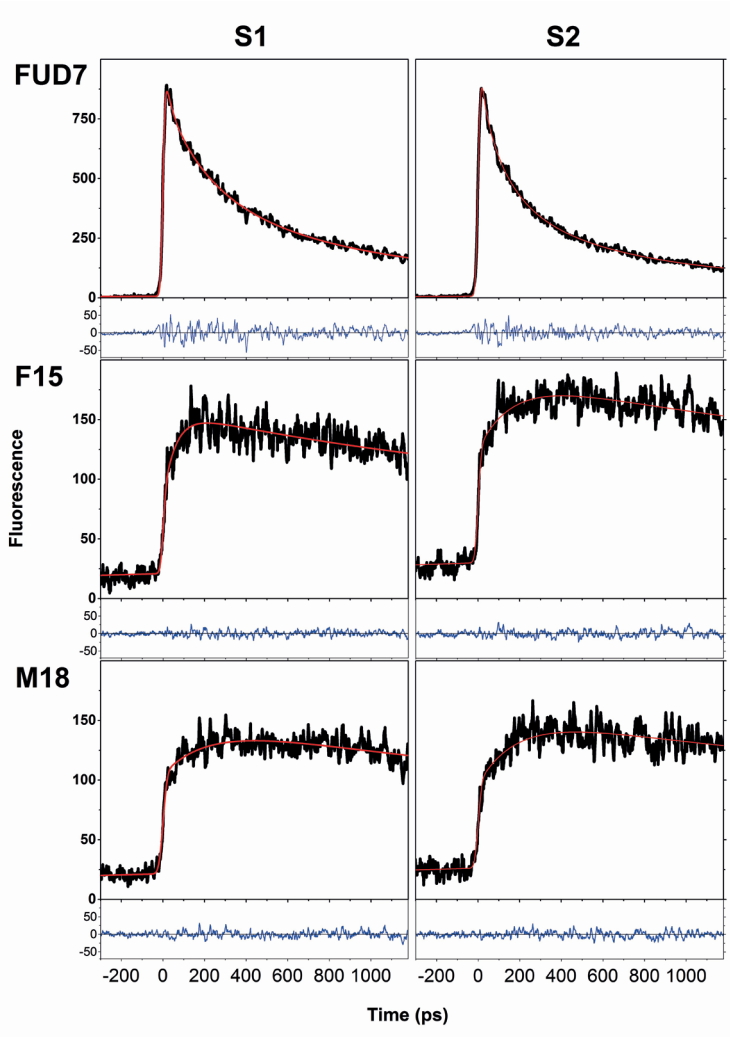

Figure S3.11 Fluorescence decay (black) measured at 77 K in FUD7 at 681 nm and in F15 and M18 at 715 nm. Global analysis performed in 670-683 nm for FUD7 and in 710-730 nm for F15 and M18 gives the fit (red) and residues (blue). Each strain and each state (S1 or S2) was analyzed independently and scaled using a scaling number obtained in global analysis of the full spectrum.

Reversibility of state transitions and the state of the F15 and FUD7 cells under growth conditions

Independent of the measurements reported in the main text, time-resolved fluorescence at 77 K was measured in the F15 cells and in the FUD7 cells (i) directly upon sampling from the culture flask, (ii) upon subsequent incubation of the remaining cells under S2 conditions, (iii) upon further incubation of the remaining cells under S1 conditions. Decay-Associate

Spectra characterizing these subsequent measurements are depicted in Figure S3.12 and are in line with the ones reported in Figure 4 in the main text. A difference observed on the short time-scale (first DAS) is most probably caused by the fact that the results reported in Figure S3.12 were collected with a lower time resolution (≈ 25 ps) than the data reported in Figure 4 (≈ 22 ps).

The results in Figure S3.12 show that S2 is reversible to S1, both in F15 and in FUD7. We observe moreover that under applied growth conditions (described in Materials and Methods of the main text) the extent of excitation energy transfer towards Lhca in the PSI-deficient cells of F15 is in between the extent observed for the S1- and S2-adapted cells of this mutant. On the other hand the untreated PSII-deficient cells of FUD7 show excitation energy kinetics similar to S1-adapted cells of FUD7.

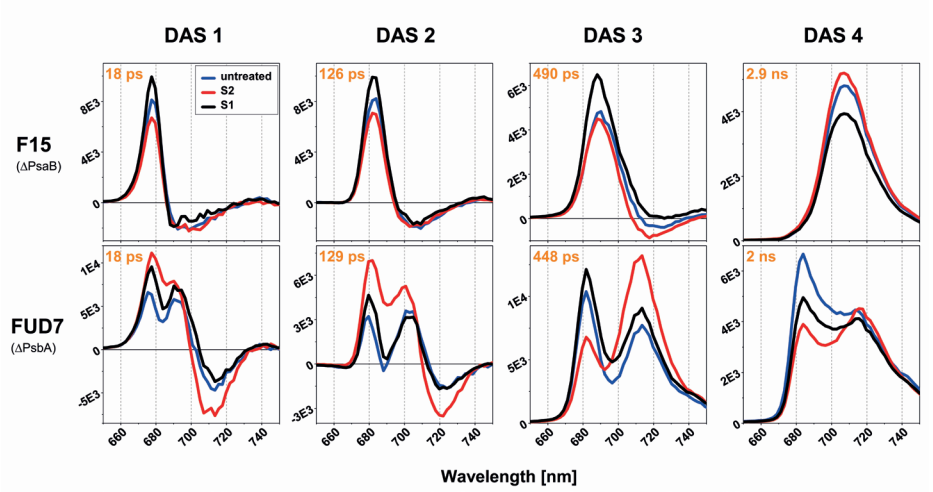

Figure S3.12 Decay-Associated Spectra (DAS) resulting from global analysis of 77 K time-resolved fluorescence measured in *C.r.* F15 and FUD7 cells directly upon sampling from culture flask ('untreated', blue), upon further incubation of the remaining cells under S1 conditions (black) and upon further incubation of the remaining cells under S1 conditions (red). Applied growth conditions and induction of state transitions were as described in Materials and Methods of the main text.